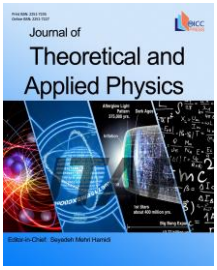

J. Theor. Appl. Phys., 2026; 20(4): 369-386

Journal of Theoretical and Applied Physics (JTAP)

https://doi.org/10.57647/jtap.2026.2004.04

Research Article

Breakthrough 31.25% Efficiency in Lead-Free Double Perovskite Tandem Solar Cells: A Novel $Cs_2AgBi_{0.75}Sb_{0.25}Br_6/CsSnI_3$ Design via SCAPS-1D Simulation

Sarowr Basm Almahsen*, Ghaleb Ali Al-Dahash

Laser Physics Department, College of Science for Women, University of Babylon, Hilla, Iraq

***Corresponding author:** sarowr.almahsen.850.csg@student.uobabylon.edu.iq

Article History:

Received:
08 January 2026

Revised:
11 February 2026

Accepted:
30 March 2026

Published in Issue:
31 August 2026

Abstract

This study examines lead-free double perovskite-based devices utilizing SCAPS-1D software simulations. The top cell in the perovskite structure studied here is a wide-bandgap double perovskite $Cs_2AgBi_{0.75}Sb_{0.25}Br_6$ (1.8 eV). In comparison, the bottom cell, made of $CsSnI_3$, has a band gap of 1.4 eV. This work proposes and simulates a unique solar cell design that $Cs_2AgBi_{0.75}Sb_{0.25}Br_6$ and $CsSnI_3$ perovskite as the primary absorber layer, tin oxide (TiO_2) as the electron transport layer (ETL), and Cu_2O as the hole transport layer. In order to optimize power conversion efficiency (PCE) under standard test conditions (AM1.5G, 1000 W/m^2, 300 K), the thicknesses of the Cu_2O HTL, the $CsSnI_3$ bottom absorber, and the $Cs_2AgBi_{0.75}Sb_{0.25}Br_6$ top absorber will be optimized. The $Cs_2AgBi_{0.75}Sb_{0.25}Br_6/CsSnI_3$ structure exhibits significant spectrum absorption, resulting in a Jsc of 31.3560mA/cm^2 and a 31.25% efficiency at 300 K. Interfacial recombination, on the other hand, lowers F.F. to 88.70% and Voc to 1.123V, both of which are below the theoretical maximum. The findings show that the stability and toxicity problems of widely utilized $Cs_2AgBi_{0.75}Sb_{0.25}Br_6$ based PSCs may be resolved by lead-free double perovskites.

Keywords: Double Perovskite, $Cs_2AgBi_{0.75}Sb_{0.25}Br_6$ /$CsSnI_3$, New architecture, Simulation, SCAPS-1D

Cite this article: Almahsen, S. B., Al-Dahash, Gh. A., (2026). Breakthrough 31.25% Efficiency in Lead-Free Double Perovskite Tandem Solar Cells: A Novel $Cs_2AgBi_{0.75}Sb_{0.25}Br_6/CsSnI_3$ Design via SCAPS-1D Simulation. *J. Theor. Appl. Phys.*, 20(4), 369-386. https://doi.org/10.57647/jtap.2026.2004.04

1. Introduction

Renewable energy sources, particularly solar power, are a viable long-term answer to the world's energy demands. The effective application of these technologies can greatly reduce the harmful environmental consequences of the traditional coal and power sectors. One important technical development in the fight against the effects of the fossil fuel industry on global climate change is the development of high-performance, reasonably priced solar panel technology [1]. Over the past 10 years, hybrid solar cells based on inorganic and organic metal halide perovskites (PSCs) have shown impressive performance gains. Significant progress in solar technology has been made as a result of these advanced systems' power conversion efficiency surpassing 22% [2]. One of the notable features of hybrid perovskite materials is their narrow bandgaps [3]. Perovskite materials' high absorption coefficients, extended charge carrier lifetimes, and tunable band adaptability enable them to be integrated into a wide range of solar structures, providing versatility in design and application. The continued development of perovskite-

based solar cell technology represents a significant step toward sustainable energy solutions. This development is compatible with global initiatives to reduce dependency on fossil fuels and develop more environmentally friendly energy generation systems [4, 5]. Ongoing research and development in this field helps to achieve the ultimate goal of creating efficient, cost-effective, and sustainable energy systems for future generations [6].

This is owing to the fact that photons with energies less than the band gap energy (Eg) go unabsorbed, but photons with energies greater than Eg encounter thermal losses, resulting in energy waste. Tandem solar cells are an excellent way to overcome this issue.

Tandem solar cells have several layers with various band gaps, which allows them to absorb photons of varying energy [7, 8].

Tandem multi-junction solar cells, composed of layers with varied band-gap energies, can enhance efficiency by using different energy regions of the sun's spectrum. A low bandgap bottom cell absorbs in the longer wavelength region of the solar spectrum, while a big bandgap top cell absorbs the short wavelength (high energy) portion. This combination makes up tandem solar cells. As a result, the Shockley-Queisser limit of a tandem solar cell is greater at 45% [9].

Tandem solar cells have been experimentally realized since 1978, with a device made of AlGaAs/GaAs achieving a PCE of around 9% [10].

Despite the extraordinary capabilities of the perovskite layer, the presence of the hazardous element lead (Pb) and the instability of the perovskite will limit its commercial viability. This limitation has drawn the researchers' attention to the creation of lead-free perovskite solar cells [11].

Lead has been replaced by either heterovalent elements such as Sb and Bi, or homovalent elements such as Sn, Ge, and Cu [12].

A three-dimensional double PVSK structure of the type A2B+B+3X6 has been created recently, in which monovalent and trivalent metal cations occupy B+ and B+3, respectively.

An appealing candidate material for photovoltaic and photovoltaic applications, the double PVSK A2B+B+3X6 structure provides enhanced stability and desired electrical characteristics [13, 14, 15].

$Cs_2AgBiBr_6$ stands out among these double perovskites for having similar optoelectronic features to lead-based perovskites, such as a 3D structure, a long carrier lifespan, and a relatively small carrier effective mass, as well as good stability and minimal toxicity. Moreover, Cs2AgBiBr6 single crystals exhibit remarkable sensitivity to X-rays (detectable dose rate of 59.7 n Gyair s−1), and $Cs_2AgBiBr_6$ solar cells have so far produced enhanced PCE of > 3% [16, 17].

$Cs_2AgBiBr_6$ has a long radiative photoluminescence lifespan, a long charge diffusion length, good defect tolerance, and higher stability under ambient settings when compared to conventional lead halide perovskites, despite having an indirect bandgap [18, 19, 20]. we used $CsSnI_3$ for the bottom cell due to its advantages. The inorganic $CsSnI_3$ perovskite has received significant attention due to its optical and electronic properties, improved thermodynamic stability, and low binding energy [21, 22]. However, the reported PCE value remained low (less than 10%), providing ample scope for further research expansion in the photovoltaic field. It has been demonstrated that $CsSnI_3$ perovskite can be grown by fusion annealing at a melting point of 451 °C, exhibiting high thermodynamic stability [21]. This study aimed to construct and optimize a lead-free, all-inorganic multilayer solar cell using an FTO/TiO_2/ $Cs_2AgBi_{0.75}Sb_{0.25}Br_6$ /$CsSnI_3$/Cu_2O structure. Simulations were performed using SCAPS-1D software.

The study focused on determining how the thickness of the bottom absorber made of $CsSnI_3$ and the defect density (N_t) in the top cell made of $Cs_2AgBi_{0.75}Sb_{0.25}Br_6$ affect the device performance.

The study used numerical simulation under AM1.5G light to develop an optimized design with 600 nm top and 900 nm bottom absorber layers, achieving a high energy conversion efficiency of 31.25%. The lead-free tandem design demonstrates significant potential, as evidenced by its high fill factor (FF) of 88.70%, short-circuit current density (Jsc) of 31.356 mA/cm², and open-circuit voltage (Voc) of 1.123V at 300 K.

2. Materials and methods

2.1. $CsSnI_3$/ $Cs_2AgBi_{0.75}Sb_{0.25}Br_6$ Perovskites: Material Properties and Applications

The Figure (Figure 3), the current density-voltage (J-V) plot, Voc, Jsc, fill factor (FF), and PCE of a $CsSnI_3$/ $Cs_2AgBi_{0.75}Sb_{0.25}Br_6$ absorber were evaluated using the SCAPS-1D numerical simulation tool [23, 24].

Table 1 summarizes each parameter utilized in the simulation. The simulations for each device (AM 1.5 G illumination; 100 mW/cm²; temperature = 300 K) were run with the SCAPS-1D program, created by Professor Marc Burgelman of Belgium [24].

The thickness of the absorber layer, HTL, and ETL were all calculated. Fluorinated tin oxide (FTO) serves as the anode, or front contact. It is a thin-film inorganic transparent conductive oxide that is both optically and

electrically transparent. This kind exhibits n-type conductivity and a broad band gap. 4.4 eV is the anticipated work function [25]. As our hole transport layer (HTL), we have added Cu_2O to facilitate the movement of the positive charge carriers.

The bandgap of Cu_2O is 2.17eV [26]. The thickness of the ETL, the initial layer in the PSC through which light travels, significantly affects efficiency.

A model of the Perovskite solar cell structure's optical performance has been created. Reducing the thickness of the TiO_2 layer to 30 nm might result in moderate increases, according to modeling of the perovskite solar cell. Consequently, the photocurrent would rise. This project's primary components were the simulations and examinations of the upper sub-cell's photovoltaic characteristics. In the upper sub-cell of a single tandem solar cell, a perovskite absorber $Cs_2AgBi_{0.75}Sb_{0.25}Br_6$ with a band gap of (1.8 eV) was employed (Figure 1).

In the lower sub-cell, the transmission wavelengths were absorbed by a narrow band gap perovskite absorber $CsSnI_3$ (1.41 eV) (Figure 2).

Last but not least, the design program SCAPS_1D (3) was used to simulate the tandem solar cell, joining the top and lower sub-cells to optimize the utilization of the full solar spectrum and attain a greater energy conversion efficiency under normal circumstances (Figure 1).

Table 1. Layer-specific parameters used in SCAPS-1D simulations

Parameters	FTO	TiO_2	$Cs_2AgBi_{0.75}Sb_{0.25}Br_6$	$CsSnI_3$	Cu_2O
Band Gap (eV)	3.5	3.2	1.8	1.4	2.17
Electron affinity (eV)	4	3.9	3.98	3.9	3.2
Dielectric permittivity	9	10	10	9.93	7.11
CB effective density of states (1 cm-3)	2.2×10^{18}	2.2×10^{18}	1×10^{16}	1×10^{19}	2.02×10^{17}
VB effective density of states (1 cm-3)	1.8×10^{19}	1.8×10^{19}	1×10^{16}	1×10^{18}	1.10×10^{19}
Electron thermal velocity (cm S-1)	1×10^{7}	1×10^{7}	1×10^{7}	1×10^{7}	1×10^{7}
Hole thermal velocity (cm S-1)	1×10^{7}	1×10^{7}	1×10^{7}	1×10^{7}	1×10^{7}
Electron mobility (cm2 VS-1)	20	100	1.620	1.5	200
Hole mobility (cm2 VS-1)	10	25	1.010	5.85	80
Shallow uniform donor density ND (1 cm-3)	2×10^{18}	1×10^{19}	1×10^{9}	0	0
Shallow uniform acceptor density NA (1 cm-3)	0	0	1×10^{9}	1×10^{17}	1×10^{19}
Defect density (Nt)	1×10^{15}	1×10^{15}	1×10^{14}	1×10^{14}	1×10^{15}
References	[27]	[27]	[28]	[29]	[27]

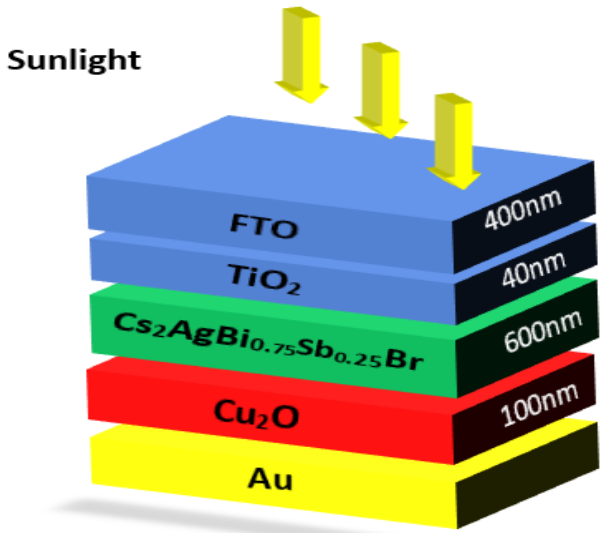

Figure 1. Design of a perovskite solar cell from $Cs_2AgBi_{0.75}Sb_{0.25}Br_6$ (top sub cell)

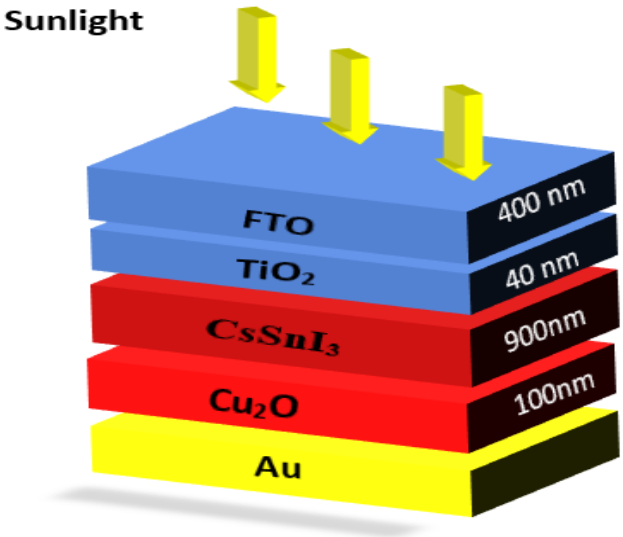

Figure 2. Design of perovskite $CsSnI_3$ solar cell (bottom sub cell)

10.57647/jtap.2026.2004.04

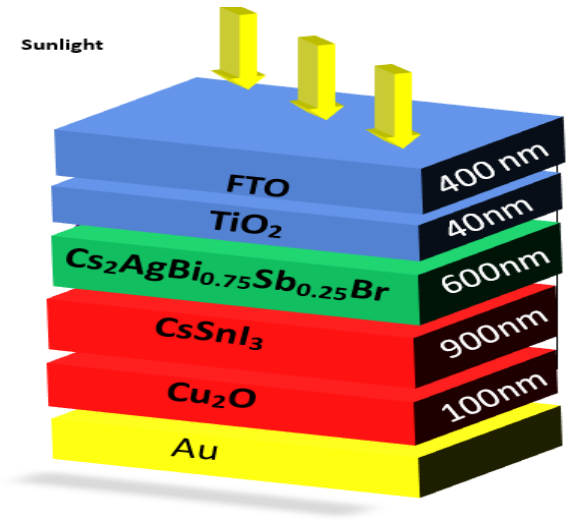

Figure 3. Schematic of the planned tandem solar cell FTO/TiO_2/ $Cs_2AgBi_{0.75}Sb_{0.25}Br_6$ (1.8eV)/$CsSnI_3$ (1.40eV)/Cu_2O/Au

4. Results and discussions

4.1. Design 1: $Cs_2AgBi_{0.75}Sb_{0.25}Br_6$ (Top Sub-Cell)

In this investigation, the fault density in the top layer was adjusted to see how it influenced the solar cell. The absorber layer defect density (Nt) ranged between 1E12 and 1E18.

As shown in Figure 4, raising Nt caused a considerable decline in performance characteristics. The findings revealed the effect of (Nt) on eta, FF, Voc, and Jsc. The efficiency peaked at 26.14% at 1E12 and then fell as fault density increased to 18.01% at 1E18. Following that, the remaining performance metrics (Voc, Jsc, and FF) were dropped.

The loss in solar cell efficiency happens as the recombination process grows while the diffusion length of charge carriers decreases, resulting in lower simulation performance.

As a result, the ideal defect density was discovered around 1E14, where charge carrier diffusion lengths are long and recombination occurs seldom. A solar cell's efficiency is mostly determined by the defect density and thickness of the absorber layer. The top layer's ideal thickness, 600nm, was employed with an efficiency of 26%.

4.2. Design 2: $CsSnI_3$ (Bottom Sub-Cell)

According to this study, because of its cheap cost, high efficiency, and remarkable thermal stability, $CsSnI_3$ is a potential lead-free material that holds promise as a lead-based material alternative in the development of environmentally friendly PSCs. tandem systems or as an efficient single-junction material, thus, forming it as a bottom cell absorber will be beneficial. As shown in (Figure 2), $CsSnI_3$ serves as the absorber layer in the intended PSC structure (FTO/TiO_2/$CsSnI_3$/Cu_2O/Au) due to its capacity to absorb light. The PV properties are significantly impacted by this capacity.

The PSC structure employs Cu_2O as the HTL, TiO_2 as the ETL, and fluorinated tin oxide (FTO) and gold (Au) as the back connection.

We utilized gold (Au) due to its high work function, which allows the creation of an Ohmic contact with the p-type HTL (Cu_2O), decreasing the Schottky barrier and reducing contact resistance and voltage losses. Its maximum efficiency is 31.16 % at 900 nm absorber thickness, as summarized in Table 2. At 900 nm, the Jsc increases to 31.39mA/cm2. However, as thickness increases, the Voc decline somewhat (1.14 V → 1.12 V), while the FF increases from (87.88% → 88.45%) (Figure 5, Table 2). According to [30, 31], the decrease in Voc may be due to an increase in recombination rate as thickness increases. The quantum efficiency (QE) of the bottom cell of CsSnI3, which is studied in the wavelength range of 300–900 nm, is displayed in Figure (6a). It is found that the quantum efficiency (QE) of the device rises throughout the wavelength region at 400 nm as the thickness of $CsSnI_3$ increases. Quantum efficiency was enhanced by increased $CsSnI_3$ thickness.

Figure (6b) displays the EBD of the bottom subcells under zero bias conditions. As explained, for the FTO/TiO_2/$CsSnI_3$/Cu_2O perovskite solar cell with a $CsSnI_3$ absorber layer thickness of 300 nm to 900 nm, increased light absorption increases the short-circuit current density, improving the power conversion efficiency (31.16%).

Increasing the thickness of the absorber layer does entail some trade-offs, including a slight decrease in the open-circuit voltage and fill factor, likely due to higher charge carrier recombination in the thicker films.

These results highlight the importance of selecting the appropriate thickness for the absorber layer in the

optimization process of achieving peak performance from perovskite solar cells. For further information, we may provide:

1- Improved Light Absorption and Current Generation: Increasing the thickness of the $CsSnI_3$ layer from 300 nm to 900 nm boosts its ability to absorb more light photons across a larger spectrum. This is plainly demonstrated in Figure (6a), which demonstrates that the device's Quantum Efficiency (QE) rises as the thickness increases over the 300-900 nm wavelength range. A larger absorber layer has a longer optical path, so more photons are caught and transformed into electron-hole pairs. The Short-Circuit Current Density (Jsc) increases significantly, reaching 31.39507mA/cm² at 900 nm (Figure 5e).

2- Peak Efficiency at Optimal Thickness: The combined impact of the soaring Jsc and the still-high voltage levels resulted in a peak Power Conversion Efficiency (PCE) of 31.16% at 900 nm (Figure 5b). This demonstrates that for this specific cell design, 900 nm marks the sweet spot where the gains in current balance the modest voltage losses.

3- The Thickness Trade-Off: Voltage and Fill Factor Loss: However, increasing the thickness has downsides. Figures 5c and 5d indicate that the Open-Circuit Voltage (Voc) and Fill Factor (FF) undergo a minor but continuous decline as the $CsSnI_3$ layer becomes thicker.

The Voc decreases from ~1.147V to 1.122V while the FF decreases from ~87.88% to 88.45%.

As previously stated, this is due to an increase in charge carrier recombination rate in thicker films. In a thicker absorber, photogenerated electrons and holes must travel a greater distance to reach their respective contacts (ETL and HTL), increasing the likelihood of them recombining before being collected.

This recombination loss is expressed as a decrease in Voc and FF. The band diagram in Figure 6b illustrates the energy landscape that facilitates this charge transport and recombination.

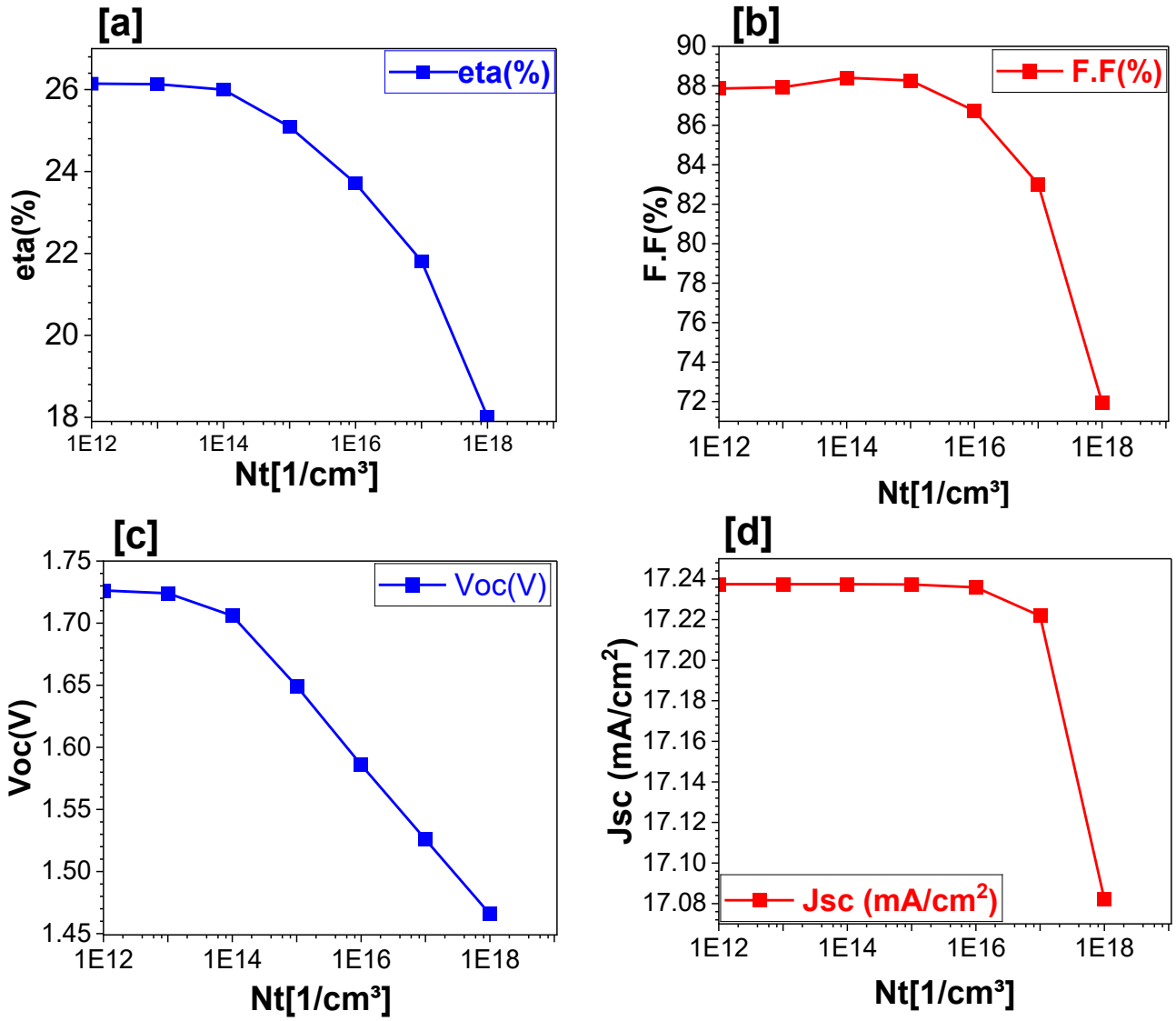

Figure 4. Changes in PSC performance parameters as absorber layer defect density varies. a) Eta, b) F.F., c) Voc, and d) JSC

10.57647/jtap.2026.2004.04

Table 2. Photovoltaic parameters of FTO (400nm)/TiO_2 (40 nm)/ $CsSnI_3$(300-900 nm)/Cu_2O (100 nm) at 300 K°

Thickness(nm)of $CsSnI_3$	eta (%)	Voc(V)	Jsc (mA/cm^2)	F.F(%)	V_mpp(V)	J_mpp (mA/cm^2)
300	25.87175	1.14734	25.65733	87.8865	1.04053	24.86407
400	27.96145	1.14145	27.80823	88.09059	1.03662	26.97364
500	29.23032	1.13624	29.15464	88.23831	1.03299	28.29685
600	30.03185	1.13181	30.03838	88.33492	1.02971	29.16543
700	30.5592	1.12811	30.64472	88.39675	1.0267	29.76451
800	30.91729	1.12494	31.07742	88.4359	1.024	30.19255
900	31.16467	1.12217	31.39507	88.45935	1.02158	30.50628

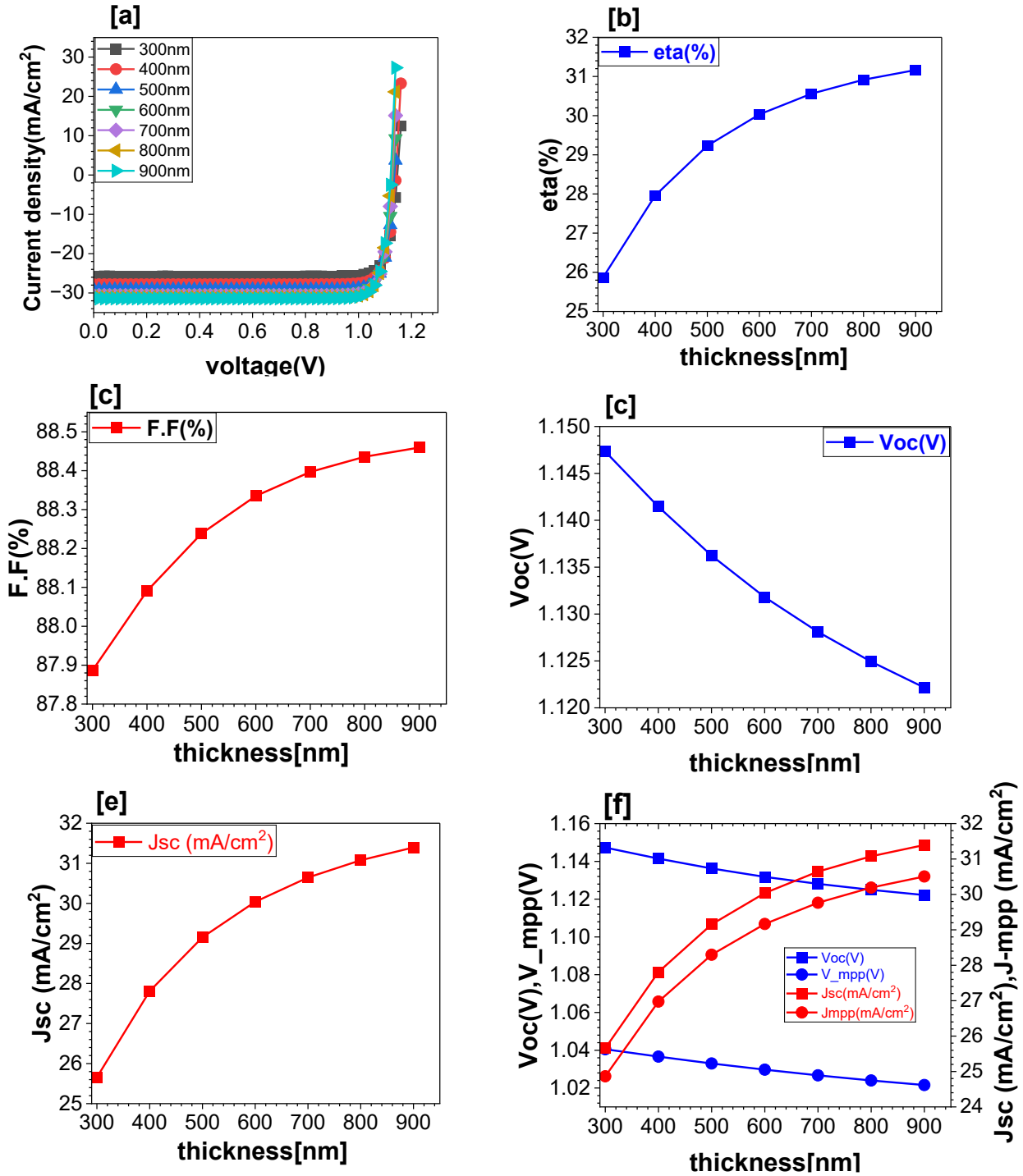

Figure 5. Effects of perovskite Thickness(nm) (bottom sub cell) on device performance: (a) J-V curves (b)eta (%), (c) F.F, (d)Voc, (e) Jsc, (f) Vmpp, and Jmpp

10.57647/jtap.2026.2004.04

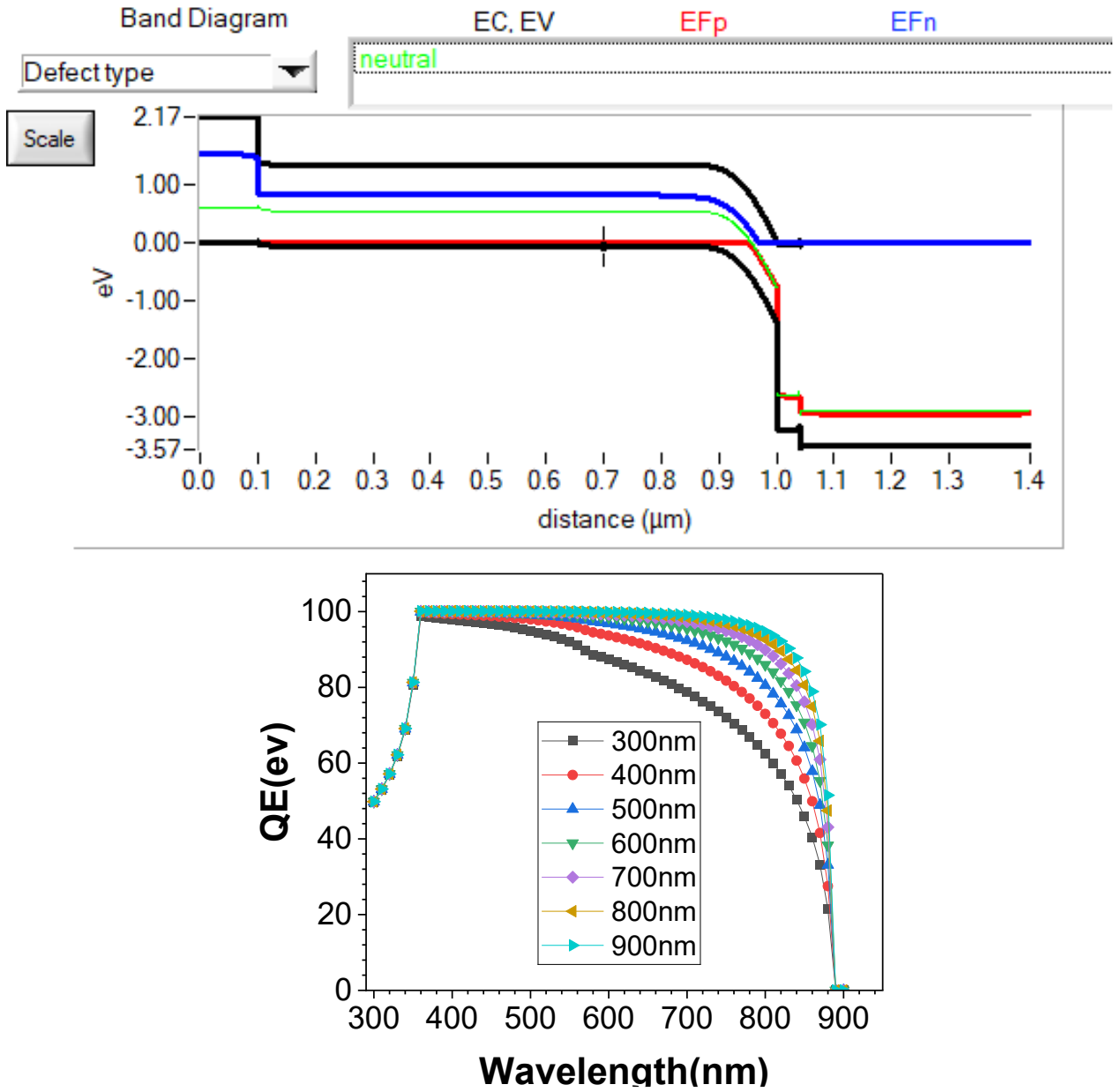

Figure 6. (a) Quantum efficiency for absorber thickness. (b) The independent top cell's energy band diagram (bottom sub cell)

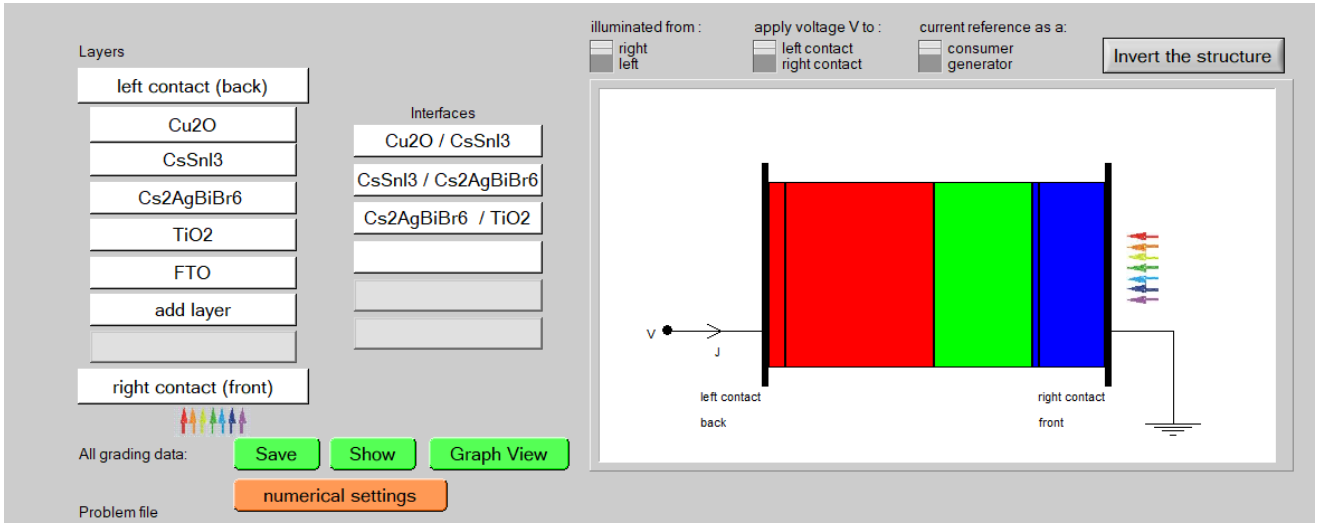

Figure 7. Schematic diagram of the designed tandem solar cell FTO/TiO_2/ $Cs_2AgBi_{0.75}Sb_{0.25}Br$ (1.8eV)/$CsSnI_3$ (1.40eV)/Cu_2O/Au

10.57647/jtap.2026.2004.04

4.3. Design 3: Tandem Cell ($Cs_2AgBi_{0.75}Sb_{0.25}Br_6$/ $CsSnI_3$)

The Figure 7 depicts a simulated two-terminal tandem configuration: (FTO/TiO_2/ $Cs_2AgBi_{0.75}Sb_{0.25}Br_6$ (1.8ev)/$CsSnI_3$/Cu_2O). In this configuration, the upper cell with a broad bandgap filters the solar spectrum, allowing low-energy photons to reach the lower $CsSnI_3$ layer. The thicknesses of the two absorption layers were tuned to achieve current matching, which is required for tandem devices, with the absorber layer thickness significantly affecting efficiency and device performance, consistent with [32, 33]. While increasing thickness enhances photon absorption and short-circuit current density (Jsc), the best balance was found at 600 nm for the upper absorption layer and 900 nm for the bottom absorption layer. At these dimensions, and with a tunnel recombination junction (TRJ) at the interface, the device provides realistic and physically consistent performance. After fixing the thickness of the upper at 600 nm and lower absorption layers at 900 nm and the temperature at 300 K, the current-voltage characteristics were shown in Figure 8. The results were as follows: η 31.25%, FF 88.70%, J_{SC} 31.356 mA/cm², and V_{OC} 1.123 V. Figure 9 shows the relationship between the incident light wavelength and the external quantum efficiency (EQE). Quantum efficiency is defined as the proportion of charge carriers collected from incident photons of a specific wavelength or energy. A significant increase in the external quantum efficiency was observed at wavelengths between 300 and 650 nm. The results for the external quantum efficiency showed an improvement with increasing thickness of the $CsSnI_3$ and $Cs_2AgBi_{0.75}Sb_{0.25}Br_6$ layers.

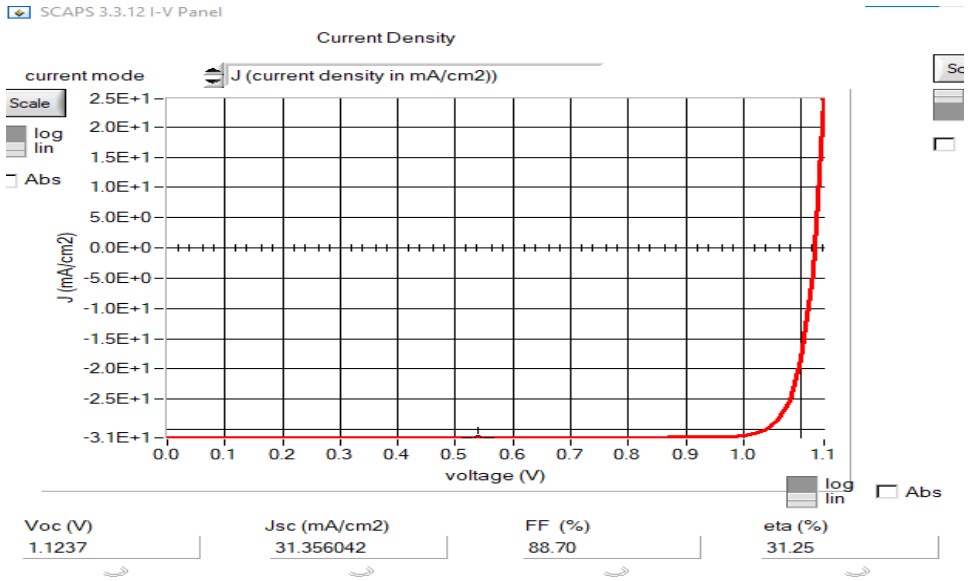

Figure 8. J-V curves for different structures of perovskites

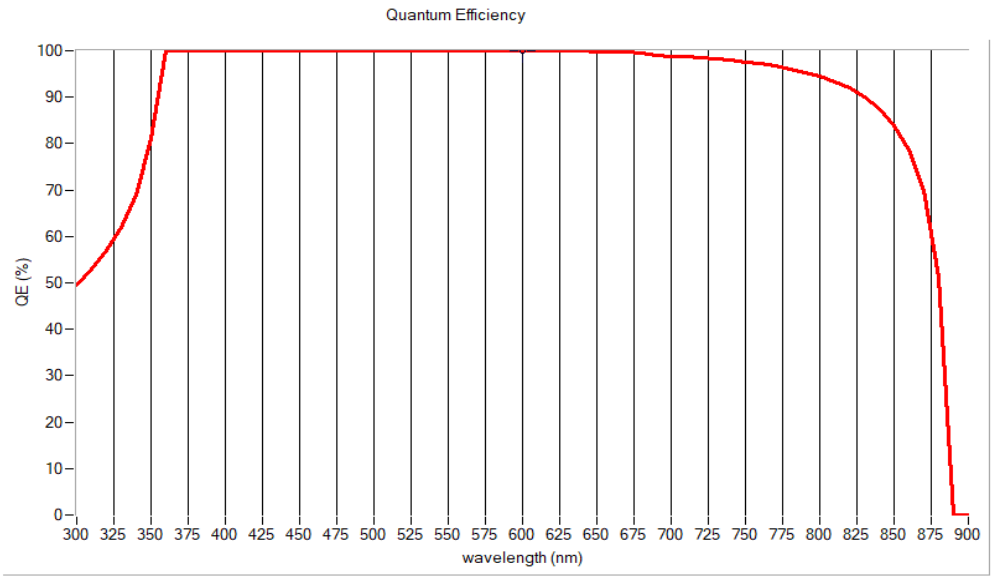

Figure 9. Shows the external quantum efficiency (EQ) of simulated devices made of several materials, including Cu2O (100nm), $CsSnI_3$ (900nm), $Cs_2AgBiSbBr_6$ (600nm), TiO_2 (40nm), and FTO (400nm)

10.57647/jtap.2026.2004.04

4.4. The effect of ETL and HTL layer thickness on device performance

A perovskite solar cell's efficiency is totally dependent on the rapid and effective extraction of charge carriers, which is carried out by the ETL and HTL. The characteristics of TiO_2 ETL and Cu_2O HTL have been thoroughly examined in order to improve the simulated device. To prevent charge recombination and facilitate easy electron transfer through the layer, an enhanced electron transport layer needs to have two characteristics: 1) high electron mobility, and 2) a lower conduction band minimum towards the adjacent layers. This will increase the overall efficiency of the device. Research supports this habit [34, 35].

4.4.1. *Thickness and Doping Concentration: Impact on ETL*

Table 3 and Figure (10) demonstrate the initial evaluation of the effect of altering TiO_2 ETL thickness from 30 to 90 nm. According to this study, increasing the thickness of the ETL results in a small but constant drop in all of the important photovoltaic metrics. The power conversion efficiency (η) falls with increasing thickness, from 31.25% at 30 nm to 31.25% at 90 nm. The open-circuit voltage (Voc), short-circuit current density (Jsc), and fill factor (F.F) all show comparable, minor declines. This study determined that the optimal thickness for the ETL is 30 nm. In an effort, the ETL was further analyzed in relation to thickness (30-90 nm) and carrier doping concentration (10^{13} cm^{-3} to 10^{19} cm^{-3}), with the results displayed in contour plots in Figure (11). The results demonstrated a close correlation between the device's performance and the doping concentration. In Figure (11a), it can be seen that for any given thickness, the efficiency shoots up with doping concentration, peaking above 31.25% at 10^{19} cm^{-3}. Figure (11b) further demonstrates this trend, showing an increase in fill factor from approximately 88.53% to over 88.96% as doping increases. This conclusion implies that higher doping may have increased the ETL conductivity, diminished the series resistance, and enhanced charge extraction. On the other side, Voc and Jsc seemed to have less dependence on doping, remaining quite stable at about 1.12V and 31.35 mA/cm², respectively (Figure 11c and 11d). Jointly from the comparison, it was confirmed that peak performance is reached with a thin and highly doped TiO_2 layer (30 nm, 10^{20} cm^{-3}). From another perspective, the observed reliance of device performance on ETL characteristics, as shown in Figure 11, may be explained by fundamental semiconductor device physics. The substantial positive link between ETL doping concentration and the device's Fill Factor (FF) and Power Conversion Efficiency (PCE) is mostly due to the reduction in series resistance (Rs). Increasing the doping concentration to 10^{20} cm^{-3} improves the electrical conductivity of the TiO_2 layer by many orders of magnitude. The extremely conductive channel reduces parasitic Ohmic voltage losses (I·Rs) during charge extraction, especially at the highest power point. The reduced resistive loss results in a squarer I-V curve, which manifests as a higher FF. As the PCE is a product of the main photovoltaic factors, The large improvement in FF is the major cause of the reported efficiency increase. In contrast, it is widely recognized that the open-circuit voltage (Voc) and short-circuit current density (Jsc) are rather insensitive to the ETL doping level. The Voc is primarily determined by the quasi-Fermi level splitting inside the absorber layers and is constrained by charge carrier recombination rates and the quality of interfacial band alignment. Our findings show that the ETL's bulk conductivity has no substantial effect on these parameters within the investigated range. Similarly, photon absorption rate in active layers governs the Jsc. The thin TiO_2 layer is transparent to the solar spectrum and has near-unity charge collecting efficiency. Improving the ETL's conductivity does not improve the amount of photogenerated carriers that can be captured.

Table 3. Photovoltaic parameters of FTO/TiO_2(30_90nm) / $Cs_2AgBi_{0.75}Sb_{0.25}Br$ (900nm)/$CsSnI_3$(900 nm)/Cu_2O (100 nm) at 300 K°

Thickness(nm)of TiO_2	eta (%)	Voc(V)	Jsc (mA/cm²)	F.F(%)	V_mpp(V)	J_mpp (mA/cm²)
30	31.25253	1.12366	31.35637	88.69981	1.02611	30.45719
40	31.25222	1.12366	31.35607	88.6998	1.02611	30.45689
50	31.25187	1.12366	31.35574	88.69978	1.02611	30.45655
60	31.25148	1.12366	31.35536	88.69977	1.02611	30.45617
70	31.25106	1.12366	31.35495	88.69975	1.02611	30.45576
80	31.2506	1.12366	31.35451	88.69973	1.02611	30.45531
90	31.2501	1.12366	31.35402	88.69971	1.02611	30.45482

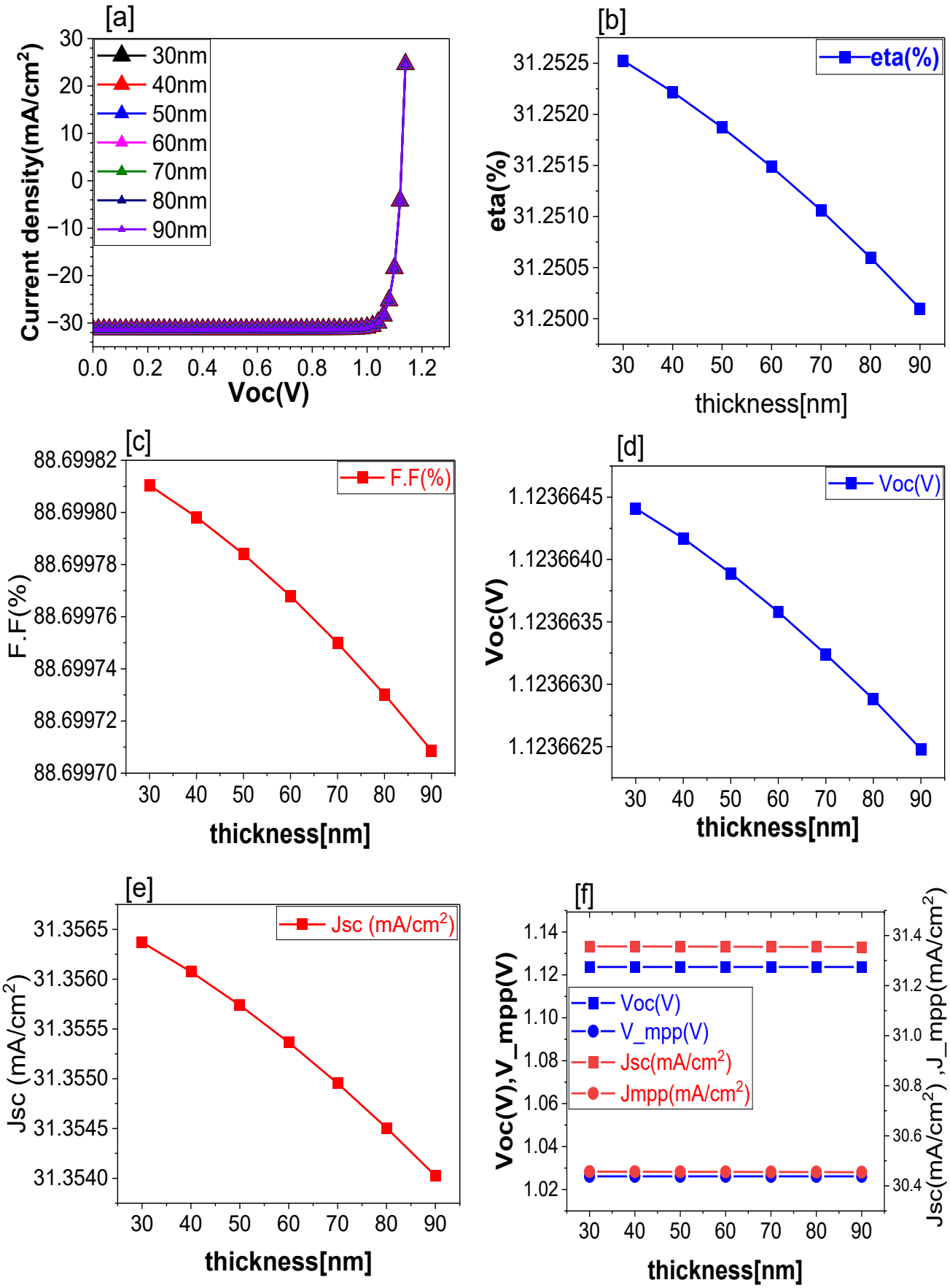

Figure 10. Effects ETL (TiO_2) Thickness (nm) on device performance: (a)J-V curves (b) eta , (c) FF, (d)Voc, (e) Jsc, (f) Vmpp and Jmpp

10.57647/jtap.2026.2004.04

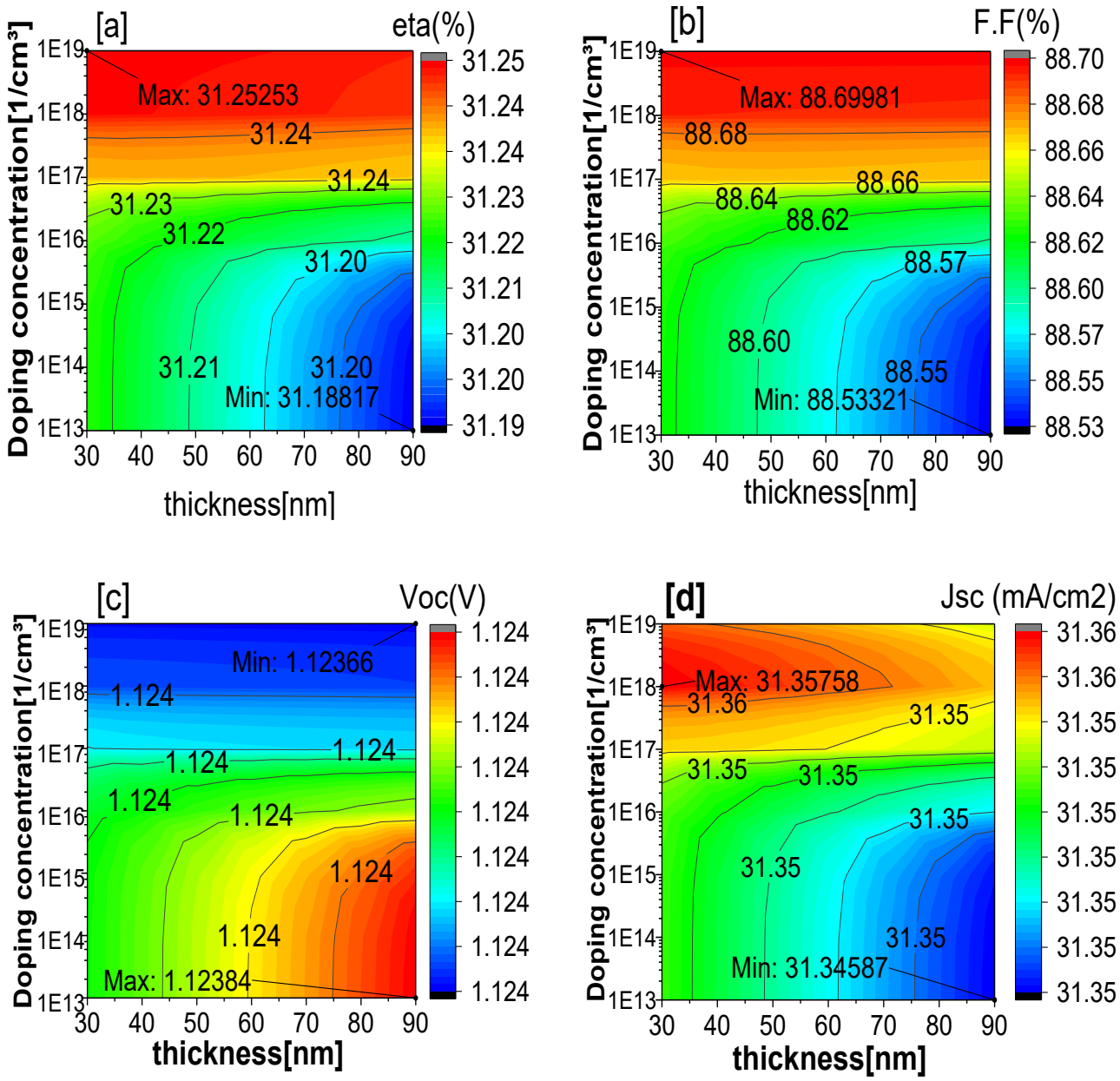

Figure 11. Impact of the ETI. (TiO_2) thickness and carrier concentration on key photovoltaic parameters: (a) eta (%), (b) F.F (%),(c)Voc(V), (d) Jsc(mA/cm^2)

Finally, a thin (30 nm) and highly doped (10^{20} cm^{-3}) TiO_2 film demonstrated perfect synergy. The high doping level assures good conductivity, which maximizes FF and PCE while minimizing resistive losses. Concurrently, the minimum thickness of 30 nm offers the shortest feasible electron transport channel while providing maximum optical transmittance to the underlying absorber layers, resulting in a high JSC.

This thickness is enough to provide a homogeneous, pinhole-free coating that successfully prevents shunt-related performance deterioration. To select the essential ETL for our device design, we compared different potential materials: inorganic TiO_2, WS_2, and CdS, as well as the organic ETL, PCBM, all at a uniform thickness of 40 nm. The results in Figure (12a), Figure (12b) and the accompanying table clearly reveal TiO_2 as the best alternative.

The TiO_2-based cell achieves 31.25% efficiency with a remarkable combination of high Jsc (31.35607mA/cm^2), Voc (1.1236V), and an amazing fill factor (88.69%). TiO_2 's wide bandgap decreases parasitic absorption, leading to a high and broad quantum efficiency spectrum.

It also has good charge transport capabilities that minimize resistive losses, as seen by its high fill factor.Although CdS performs well, PCBM and WS_2 have lower fill factors and more parasitic absorption, making them less suitable for maximum device output.

After screening several materials, TiO_2 was chosen for further optimization of thickness and doping concentration, as shown in Table 4.

10.57647/jtap.2026.2004.04

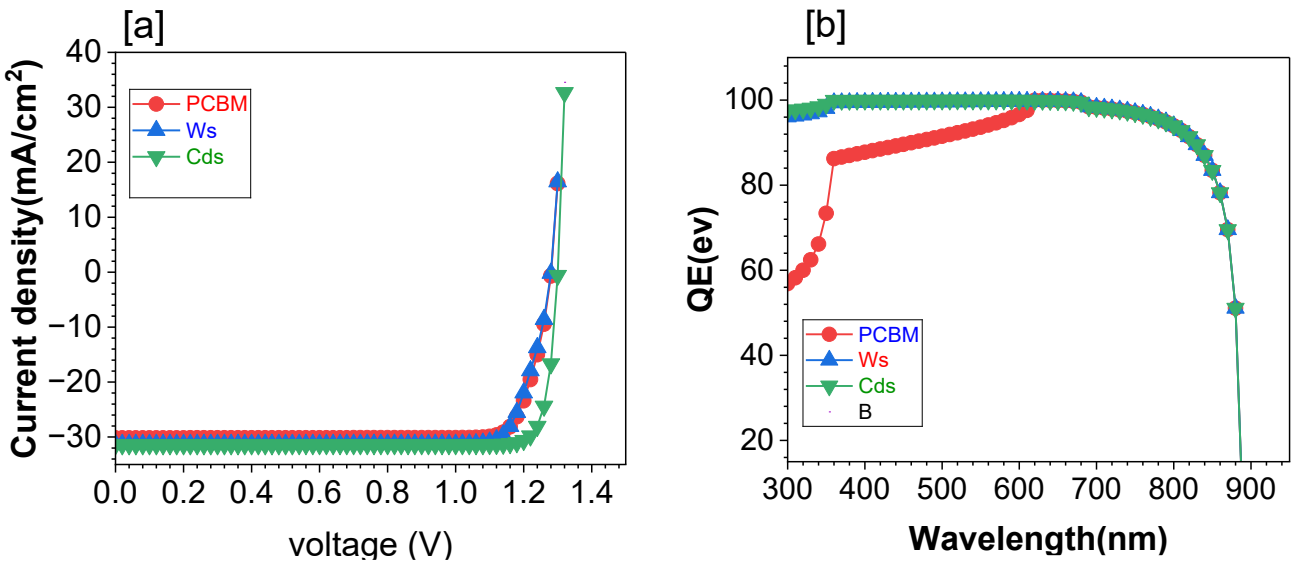

Figure 12. (a) J-V characteristics with varied ETL, (b) EQ (%)

Table 4. Shows the solar cell parameters for several ETL materials

ETL material	Jsc (mA/cm2)	Voc (V)	F.F(%)	Eta (%)
TiO2	31.35607	1.12366	88.6998	31.25222
PCBM	30.181	1.2811	86.06	33.27
Ws	31.334	1.2803	85.13	34.15
Cds	31.404	1.3004	90.00	36.76

4.4.2. *Effect of the Thickness of Hole Transport Layer (Cu_2O)*

To assess its effect on device performance, the thickness of the Cu_2O HTL was varied from 100 to 400 nm, with results recorded in the correlated table and Figure (13). The simulation demonstrates that the device is extremely resistant to HTL thickness fluctuations in this range. All four important metrics are almost unaffected: efficiency (η ≈ 31.25%), open-circuit voltage (Voc = 1.12V), short-circuit current density (Jsc ≈ 31.35604mA/cm²), and fill factor (F.F ≈ 88.69%). The insensitivity indicates that the Cu_2O layer for this specific stack of materials does a very good job of extracting holes, even at 400 nm, with very little recombination loss through the HTL. This study looks at ways to make lead-free double perovskite tandem solar cells more efficient, connecting it to recent progress in CIGS-based solar panels, and highlighting how important the thickness of the layers and reflective structures are. For instance, the reference study (by our team) [36] found that making the absorption layer thicker in CIGS/TiO_2/ZTO/ZnO/Al solar cells boosts efficiency until it reaches the best balance with the other layers, similar to what we discovered about optimizing the thickness of the $Cs_2AgBi_{0.75}Sb_{0.25}Br_6$ /$CsSnI_3$ absorber. The CIGS study achieved 24.84% efficiency by integrating a $MoSe_2$ back reflection layer, which reduced the absorption layer thickness to 0.5 µm and increased light trapping. This technique may influence comparable solutions for addressing interfacial recombination losses in perovskite tandems, as shown in Table 5. Despite facing stability issues that CIGS technology does not, perovskite-based devices provide significant advantages such as increased theoretical efficiency limits (31.25% in our tandem design) and customizable bandgaps. The CIGS work used back reflection to minimize manufacturing costs, whereas our study focuses on lead-free perovskites to address both toxicity and production costs simultaneously, revealing alternate methods to promoting sustainable solar energy. Future research might explore combining perovskite absorbers with reflective back layers to solve thickness problems and lower material costs.

Table 5. Photovoltaic parameters of FTO (400nm)/TiO_2 (40) nm)/ $Cs_2AgBi_{0.75}Sb_{0.25}Br$ (900nm)/$CsSnI_3$(900 nm)/Cu_2O (100_400 nm) at 300 K°

Thickness (nm) of Cu_2O	eta (%)	Voc(V)	Jsc (mA/cm²)	F.F (%)	Vmpp(V)	Jmpp (mA/cm²)
100	31.25217	1.12366	31.35604	88.69979	1.02611	30.45684
150	31.25218	1.12366	31.35605	88.69979	1.02611	30.45685
200	31.25219	1.12366	31.35606	88.69979	1.02611	30.45686
250	31.2522	1.12366	31.35607	88.69979	1.02611	30.45687
300	31.25221	1.12366	31.35608	88.69979	1.02611	30.45688
350	31.25221	1.12366	31.35609	88.69979	1.02611	30.45688
400	31.25222	1.12366	31.35609	88.69979	1.02611	30.45689

10.57647/jtap.2026.2004.04

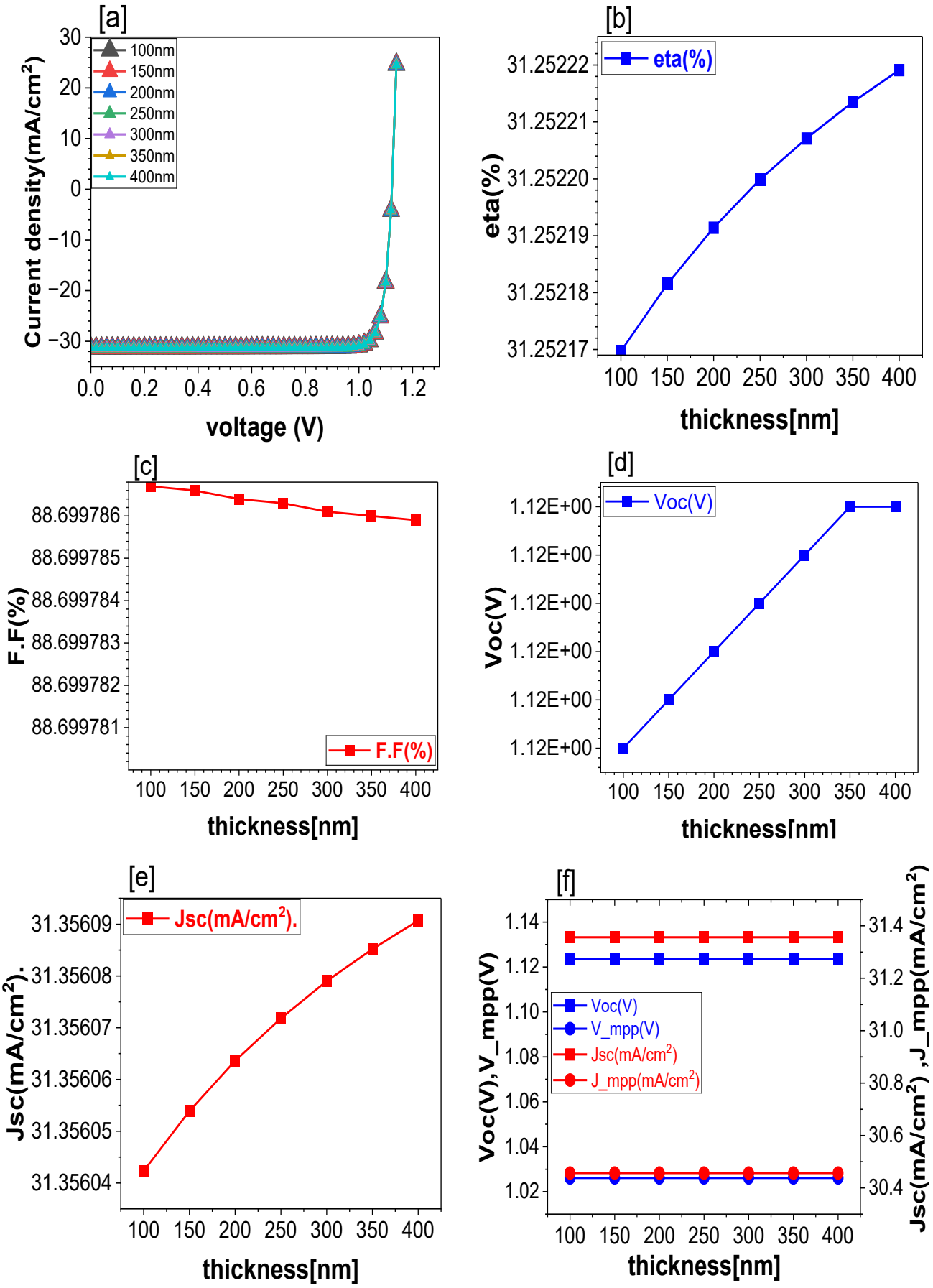

Figure 13. Effects HTL (Cu_2O) Thickness (nm) on device performance: (a) J-V curves ,(b) eta,(c) F.F, (d) Voc,(e) Jsc,(f) Vmpp and Jmpp

10.57647/jtap.2026.2004.04

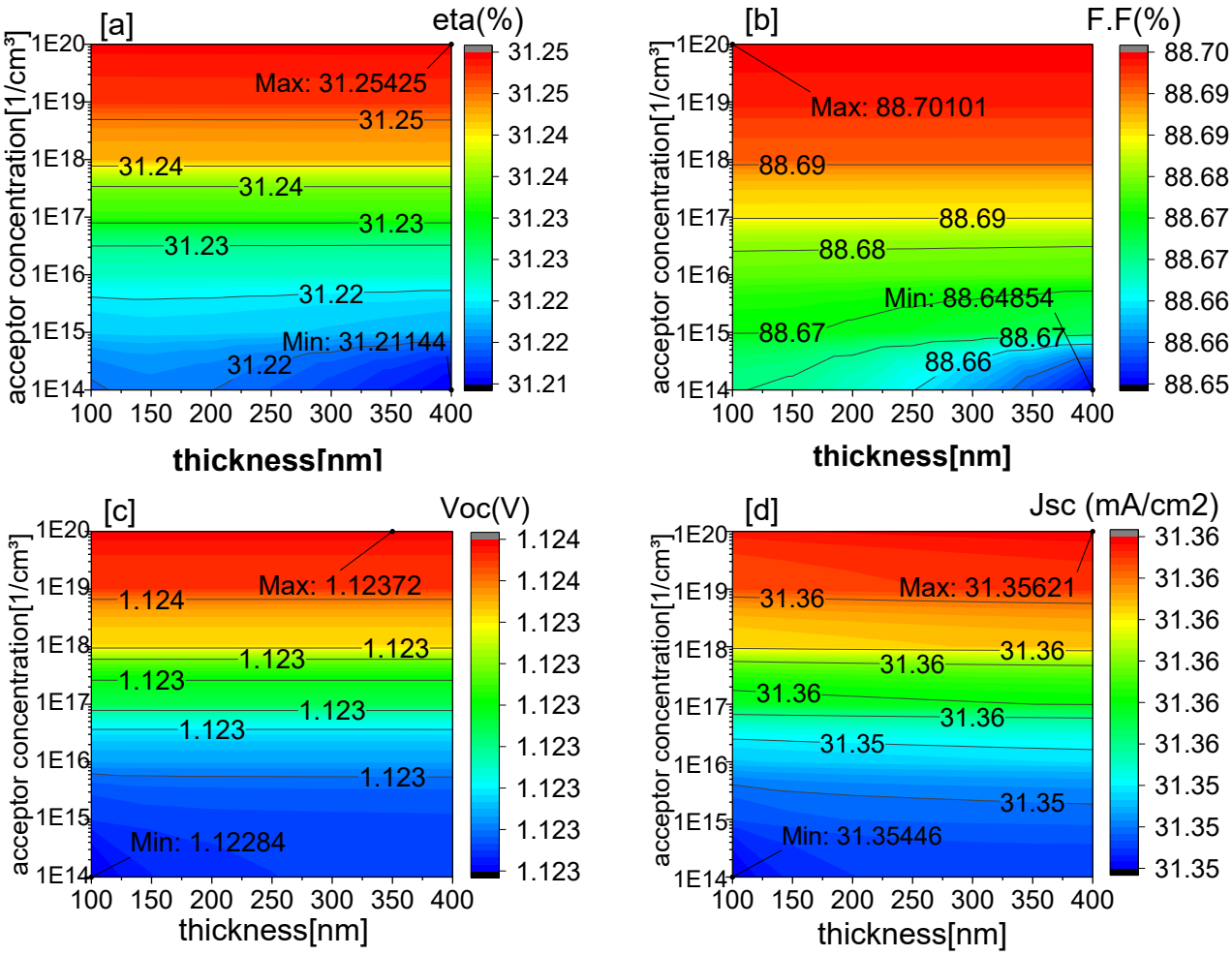

Figure 14. Impact of Cu_2O HTL thickness and carrier concentration on key photovoltaic parameters

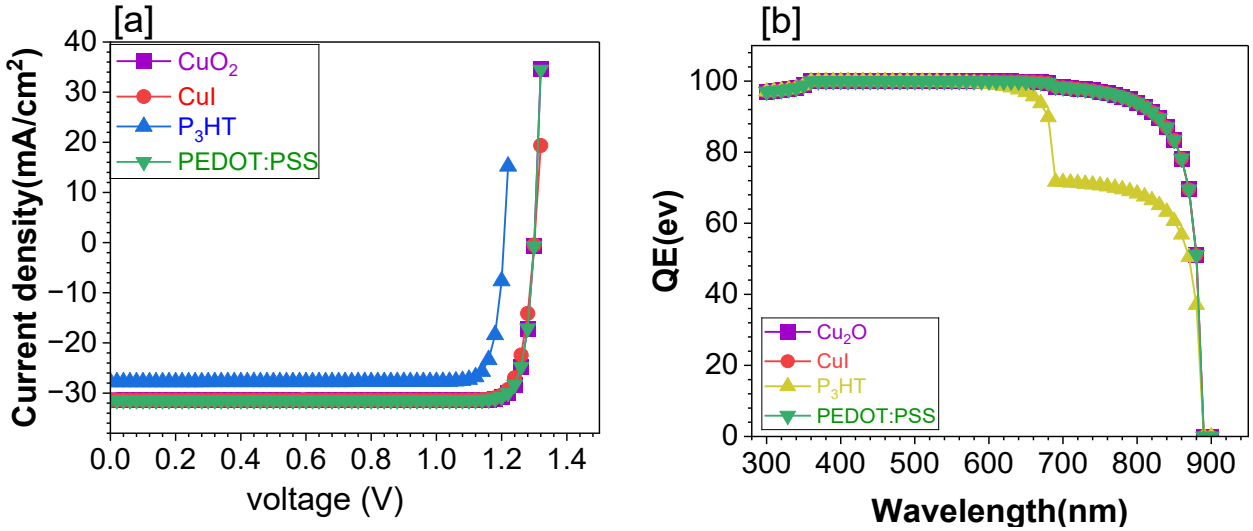

Figure 15. (a) J-V characteristics with varying HTL, (b) EQ (%)

Table 6. Solar cell properties for various HTL materials

HTL material	Jsc (mA/cm2)	Voc (V)	F.F(%)	Eta (%)
Cu_2O	31.35604	1.12366	88.69979	31.25217
CuI	31.4056	1.3006	89.49	36.55
P3HT	27.7828	1.2080	89.58	30.06
PEDOT: PSS	31.4057	1.3005	90.31	36.89

10.57647/jtap.2026.2004.04

Table 7. Compares our study to previously published results

Device structure (material system)	Voc(V)	Jsc(mA/cm^2)	F.F (%)	PCE (%)	Ref.
TiO_2/ $Cs_2AgBi_{0.75}Sb_{0.25}Br_6$/ $CsSnI_3$/Cu_2O/Au	1.12	31.35	88.69	31.25	This Work
FTO/Zn (O0.3, S0.7)/ Cs2AgBi0.75Sb0.25Br6/ V2O5/Pt	1.68	18.37	91.94	28.43	[40]
FTO/C60/Cs2AgBiBr6/MoS2/Pt	0.84	32.28	85.77	23.49	[41]
FTO/ZnO/ Cs2AgBi0.75Sb0.25Br6/ $FAMASnGeI_3$/ NiO/Ag	2.09	15.58	80.87	29.59	[42]
FTO /TiO2/ Cs2AgBi0.75Sb0.25Br6/ FASnI3/Cu2O/Au	1.1402	27.886	88.74	28.22	[43]

Tables 6 & 7 show the solar cell with a Cu_2O HTL in our work demonstrates superior performance, achieving high power conversion efficiency (PCE) of 31.25%. This is attributed to its optimal combination of a high short-circuit current density (Jsc), open-circuit voltage (Voc), and fill factor (FF).

The performance of Cu_2O is identical to PEDOT: PSS and superior to CuI and P3HT, establishing it as a highly effective hole transport material. Furthermore, as shown in the comparison table, our device's PCE of 31.25% significantly surpasses the efficiencies reported in previous studies on similar $Cs_2AgBiBr_6$-based perovskite solar cells, which typically range from ~23% to 29% (Figure 14). While some previous efforts attained a higher Voc, this was frequently at the price of a substantially lower Jsc. Our gadget properly balances all three critical parameters (Jsc, Voc, and FF), resulting in unprecedented efficiency for this material system and marking a significant development in the sector.

Figure 15 demonstrates that the Cu_2O HTL in this high-efficiency perovskite solar cell functions ideally due to a combination of physical and electrical properties. The ideal conditions for Cu_2O HTL are a thin layer (~100-200 nm) and a high acceptor concentration (>10^{18} cm^{-3}) due to the following synergistic effects:

1- Reduced Series Resistance (Rs): A thin layer physically shortens the carrier route, but a high acceptor concentration increases conductivity.

Both variables significantly lower the HTL's total series resistance, resulting in exceptional Jsc and near-ideal F.F (31.35mA/cm² and 88.69%, respectively).

2- Efficient Charge Carrier Collection: The short transit distance in a thin layer, together with the fast transport provided by high conductivity, guarantees that holes are recovered from the absorber rapidly and efficiently before they may recombine.

This reduces bulk recombination within the HTL and at the interfaces.

3- Optimal hole extraction at the interface. A highly doped Cu_2O layer makes a good charge selective contact, effectively removing holes from the perovskite without obstructing their flow maintaining a strong driving force for charge separation within the absorber.

4- Synoptic High PCE: Optimizing Jsc and F.F simultaneously while keeping a steady and high Voc results in an excellent Power Conversion Efficiency of 31.25%. The ideal Cu_2O HTL is designed to provide a highly conductive, low-resistance conduit for holes, enabling their quick and full collection. This maximizes the device's electrical output This tendency is consistent with the majority of study papers [37, 38, 39].

4.4.3. *Contextual Analysis and Future Outlook*

The research into the optimization of lead-free perovskite solar cells closely tracks advancements in the photovoltaics sector, particularly recent advances in CIGS-based devices.

An earlier evaluation of CIGS-based solar cells, for example, recommended improving the thickness of the absorber layer while simultaneously increasing efficiency to 24.84% after interfering with a $MoSe_2$ back reflection layer. Such an approach, along with other improvements in light trapping via reflective structures and stall required material thickness, could be employed for perovskite-type devices in minimizing interfacial recombination losses. Higher theoretical efficiency limits, as demonstrated by the 31.25% in our tandem design, and highly tunable bandgaps have been realized, but perovskite technology currently faces greater challenges with respect to stability. Our research aims to promote sustainable solar energy by developing lead-free perovskites to counter the toxicity of materials, providing another angle to solutions, such as using reflective layers to minimize costs of production in CIGS cells.

Future research might look at the synergistic combinations of improving lead-free perovskite absorbers with enhanced optical structures back reflectors to reach even better efficiency while using less material.

To actualize the theoretical design of our multilayer solar cell, we propose the following preparation techniques for each layer. For the TiO_2 layer, we propose using Atomic Layer Deposition (ALD) or Sputtering. TiO_2 's crystalline structure determines its hardness, which ranges from 5 to 9 GPa. Proper preparation ensures good adhesion. Perovskite absorber layers include $Cs_2AgBi_{0.75}Sb_{0.25}Br_6$, which may

be deposited by Spin-Coating for a homogenous coating, however particular hardness values are less known. Adhesion can vary but is often enhanced with surface treatments. Thermal evaporation is indicated for $CsSnI_3$, which has hardness values of 1-3 GPa and varies in adhesion depending on the substrate. The Transparent Conducting Oxide (TCO) layer should be deposited using sputtering because FTO films have high toughness and adhesion qualities. Finally, Thermal Evaporation or Sputtering is appropriate for Au metal contact, since it has a low hardness of roughly 2-3 GPa and high adherence to various substrates, especially when adhesion coatings like Cr or Ti are used. These strategies are designed to improve the performance and stability of each layer in the multilayer solar cell construction.

5. Conclusion

We model and calibrate the state-of-the-art conversion efficiencies of the independently operated $Cs_2AgBi_{0.75}Sb_{0.25}Br_6$ and $CsSnI_3$ perovskite absorber layer with bandgaps of 1.4eV and 1.8eV, respectively. Additionally, significant attempts were made to use these perovskite absorber materials to develop a tandem device that is entirely perovskite and devoid of lead. Both the top and bottom subcells' absorber layer thicknesses have been changed to meet the present matching circumstances in order to accomplish a realistic tandem operation. It was discovered that the ideal thickness for the top 600 nm and bottom cell absorber layers was and 900 nm, respectively. Under the present matching circumstance, individual cell efficiency is 26.00% (top) and 31.16% (bottom). A series (2T) connection between the top and bottom cells is used to create a tandem device. It was improved. The HTL (Cu_2O) had thicknesses of 100 nm and 400 nm, whereas the ETL (TiO2) had thicknesses of 30 nm and 90 nm. This led to improved device performance with FF (88.69%), Jsc (31.35mA/cm^2), eta (31.25%), and Voc (1.12V), respectively. This highlights the possibility of designing high-efficiency, lead-free, and environmentally friendly perovskite solar cells based on $Cs_2AgBi_{0.75}Sb_{0.25}Br_6$ and $CsSnI_3$.

Authors Contribution
All the authors have participated sufficiently in the intellectual content, conception and design of this work or the analysis and interpretation of the data, as well as the writing of the manuscript.

Availability of data and materials
Data will be made available upon reasonable request to the corresponding author.

Conflict of interests
The authors declare no conflict of interest.

References

[1] Kannan, N., & Vakeesan, D. (2016). Solar energy for future world:-A review. *Renewable and sustainable energy reviews*, *62*, 1092-1105. https://doi.org/10.1016/j.rser.2016.05.022

[2] Yang, W. S., Noh, J. H., Jeon, N. J., Kim, Y. C., Ryu, S., Seo, J., & Seok, S. I. (2015). High-performance photovoltaic perovskite layers fabricated through intramolecular exchange. *Science*, *348*(6240), 1234-1237. https://doi.org/10.1126/science.aaa9272

[3] Ge, M.; Yang, X.; Cai, B.; Pan, S.; Cui, H.; Zhang, T.; Ji, W. Naphthylmethylamine post-treatment of MAPbI3 perovskite solar cells with simultaneous defect passivation and stability improvement. *Sol. Energy* 2021, *220*, 18–23. https://doi.org/10.1016/j.solener.2021.03.016

[4] Brenner, T. M., Egger, D. A., Kronik, L., Hodes, G., & Cahen, D. (2016). Hybrid organic—inorganic perovskites: low-cost semiconductors with intriguing charge-transport properties. *Nature Reviews Materials*, *1*(1), 1-16. DOI https://doi.org/10.1038/natrevmats.2015.7

[5] Lin, Q., Armin, A., Nagiri, R. C. R., Burn, P. L., & Meredith, P. (2015). Electro-optics of perovskite solar cells. *Nature Photonics*, *9*(2), 106-112. https://doi.org/10.1038/nphoton.2014.284

[6] W. Shockley, H.J. Queisser, Detailed Balance Limit of Efficiency of p-n Junction Solar Cells, J. Appl. Phys. 32 (1961) 510–519.

[7] Amiri, S. and Dehghani, S., 2020. Design of highly efficient CZTS/CZTSe tandem solar cells. Journal of Electronic Materials, 49, pp.2164-2172. https://doi.org/10.1007/s11664-019-07898-w

[8] Elbar, M., Tobbeche, S., & Merazga, A. (2015). Effect of top-cell CGS thickness on the performance of CGS/CIGS tandem solar cell. *Solar energy*, *122*, 104-112. https://doi.org/10.1016/j.solener.2015.08.029

[9] Ragay, F. W., Marti, A., Araujo, G. L., & Wolter, J. H. (1996). Experimental analysis of the efficiency of heterostructure GaAs AlGaAs solar cells. *Solar energy materials and solar cells*, *40*(1), 5-21. https://doi.org/10.1016/0927-0248(95)00060-7

[10] Bedair, S. M., Lamorte, M. F., & Hauser, J. R. (1979). A two-junction cascade solar-cell structure. *Applied Physics Letters*, *34*(1), 38-39.

https://doi.org/10.1063/1.90576

[11] Sani, F., Shafie, S., Lim, H. N., & Musa, A. O. (2018). Advancement on lead-free organic-inorganic halide perovskite solar cells: a review. *Materials*, *11*(6), 1008. https://doi.org/10.3390/ma11061008

[12] Ijam, A. (2025). Design and Assessment of the Electrical Characteristics of Cs2AgBi0. 75Sb0. 25Br6 Perovskite Solar Cell: A Numerical Study. *Results in Engineering*, 105180. https://doi.org/10.1016/j.rineng.2025.105180

[13] Lei, H., Hardy, D., & Gao, F. (2021). Lead-free double perovskite Cs2AgBiBr6: fundamentals, applications, and perspectives. *Advanced Functional Materials*, *31*(49), 2105898. https://doi.org/10.1002/adfm.202105898

[14] Mehrabian, M., Norouzzadeh, P., & Akhavan, O. (2025). Numerical optimization of cesium tin-germanium triiodide/antimony selenide perovskite solar cell with fullerene nanolayer. *Journal of Physics and Chemistry of Solids*, *196*, 112370. https://doi.org/10.1016/j.jpcs.2024.112370

[15] Magdalin, A. E., Nixon, P. D., Jayaseelan, E., Sivakumar, M., Devi, S. K. N., Subathra, M. S. P., ... & Ananthi, N. (2023). Development of lead-free perovskite solar cells: Opportunities, challenges, and future technologies. *Results in Engineering*, *20*, 101438. https://doi.org/10.1016/j.rineng.2023.101438

[16] Pan, W., Wu, H., Luo, J., Deng, Z., Ge, C., Chen, C., ... & Tang, J. (2017). Cs2AgBiBr6 single-crystal X-ray detectors with a low detection limit. Nature photonics, 11(11), 726-732. https://doi.org/10.1038/s41566-017-0012-4

[17] Wang, B., Li, N., Yang, L., Dall'Agnese, C., Jena, A. K., Sasaki, S. I. & Wang, X. F. (2021). Chlorophyll derivative-sensitized TiO2 electron transport layer for record efficiency of Cs2AgBiBr6 double perovskite solar cells. *Journal of the American Chemical Society*, *143*(5), 2207-2211. https://pubs.acs.org/doi/10.1021/jacs.0c12786

[18] Ning, W., Wang, F., Wu, B., Lu, J., Yan, Z., Liu, X., ... & Gao, F. (2018). Long electron–hole diffusion length in high-quality lead-free double perovskite films. *Advanced Materials*, *30*(20), 1706246. https://doi.org/10.1002/adma.201706246

[19] McClure, E. T., Ball, M. R., Windl, W., & Woodward, P. M. (2016). Cs2AgBiX6 (X= Br, Cl): new visible light absorbing, lead-free halide perovskite semiconductors. *Chemistry of Materials*, *28*(5), 1348-1354. https://pubs.acs.org/doi/10.1021/acs.chemmater.5b04231

[20] Slavney, A. H., Hu, T., Lindenberg, A. M., & Karunadasa, H. I. (2016). A bismuth-halide double perovskite with long carrier recombination lifetime for photovoltaic applications. *Journal of the American chemical society*, *138*(7), 2138-2141. https://doi.org/10.1021/jacs.5b13294

[21] Zhang, T., Li, H., Ban, H., Sun, Q., Shen, Y., & Wang, M. (2020). Efficient CsSnI 3-based inorganic perovskite solar cells based on a mesoscopic metal oxide framework via incorporating a donor element. *Journal of materials chemistry A*, *8*(7), 4118-4124. https://doi.org/10.1039/C9TA11794F

[22] Hossain, M. K., Toki, G. I., Samajdar, D. P., Mushtaq, M., Rubel, M. H. K., Pandey, R., ... & Bencherif, H. (2023). Deep insights into the coupled optoelectronic and photovoltaic analysis of lead-free CsSnI3 perovskite-based solar cell using DFT calculations and SCAPS-1D simulations. *ACS omega*, *8*(25), 22466-22485. https://pubs.acs.org/doi/full/10.1021/acsomega.3c00306

[23] Burgelman, M., Verschraegen, J., Degrave, S., & Nollet, P. (2004). Modeling thin-film PV devices. *Progress in Photovoltaics: Research and Applications*, *12*(2-3), 143-153.

[24] Burgelman, M., Nollet, P., & Degrave, S. (2000). Modelling polycrystalline semiconductor solar cells. *Thin solid films*, *361*, 527-532. https://doi.org/10.1016/S0040-6090(99)00825-1

[25] Helander, M. G., Greiner, M. T., Wang, Z. B., Tang, W. M., & Lu, Z. H. (2011). Work function of fluorine doped tin oxide. *Journal of Vacuum Science & Technology A*, *29*(1). https://doi.org/10.1116/1.3525641

[26] Hossain, M. I., Alharbi, F. H., & Tabet, N. (2015). Copper oxide as inorganic hole transport material for lead halide perovskite based solar cells. *Solar energy*, *120*, 370-380. https://doi.org/10.1016/j.solener.2015.07.040

[27] N. Singh, A. Agarwal, and M. Agarwal, "Numerical simulation of highly efficient lead-free all-perovskite tandem solar cell," *Sol. Energy*, vol. 208, pp. 399–410, 2020. https://doi.org/10.1016/j.solener.2020.08.003

[28] J. Madan, R. Pandey, and R. Sharma, "Device simulation of 17.3% efficient lead-free all-perovskite tandem solar cell," *Sol. energy*, vol. 197, pp. 212–221, 2020. https://doi.org/10.1016/j.solener.2020.01.006

[29] W.-J. Yin, J.-H. Yang, J. Kang, Y. Yan, and S.-H. Wei, "Halide perovskite materials for solar cells: a theoretical review," *J. Mater. Chem. A*, vol. 3, no. 17, pp. 8926–8942, 2015. https://doi.org/10.1039/C4TA05033A

[30] Bhattarai, S., Pandey, R., Madan, J., Ahmed, F., & Shabnam, S. (2022). Performance improvement approach of all inorganic perovskite solar cell with numerical simulation. *Materials Today Communications*, *33*, 104364. https://doi.org/10.1016/j.mtcomm.2022.104364

[31] Singh, A. K., Srivastava, S., Mahapatra, A., Baral, J. K., & Pradhan, B. (2021). Performance optimization of lead free-MASnI3 based solar cell with 27% efficiency by numerical simulation. *Optical Materials*, *117*, 111193. https://doi.org/10.1016/j.optmat.2021.111193

[32] Tara, A., Bharti, V., Sharma, S., & Gupta, R. (2021). Device simulation of FASnI3 based perovskite solar cell with Zn (O0. 3, S0. 7) as electron transport layer using SCAPS-1D. *Optical Materials*, *119*, 111362. https://doi.org/10.1016/j.optmat.2021.111362

[33] Son, D. Y., Im, J. H., Kim, H. S., & Park, N. G. (2014). 11% efficient perovskite solar cell based on ZnO nanorods: an effective charge collection system. *The Journal of Physical Chemistry C*, *118*(30), 16567-16573. https://doi.org/10.1021/jp412407j

[34] Kırbıyık, Ç., Kara, D. A., Kara, K., Büyükçelebi, S., Yiğit, M. Z., Can, M., & Kuş, M. (2019). Improving the performance of inverted polymer solar cells through modification of compact TiO2 layer by different boronic acid functionalized self-assembled monolayers. *Applied Surface Science*, *479*, 177-184. https://doi.org/10.1016/j.apsusc.2019.01.268

[35] Nie, J., Zhang, Y., Wang, J., Li, L., & Zhang, Y. (2024). Recent progress in regulating surface potential for high-efficiency perovskite solar cells. *ACS Energy Letters*, *9*(4), 1674-1681. https://doi.org/10.1021/acsenergylett.4c00240

[36] Yass, A., Al-Dahash, G. A., & Abd, J. A. (2025). Optimization of absorption layer and back reflection layer thicknesses for enhanced solar cell efficiency. *Results in Optics*, 100870. https://doi.org/10.1016/j.rio.2025.100870

[37] Kundara, R., & Baghel, S. (2025). Performance optimization of CsSnI3-based perovskite solar cells using SCAPS-1D and machine learning analysis. Journal of Optics, 1-14. https://doi.org/10.1007/s12596-025-02510-3

[38] Yadav, A., Kundara, R., & Baghel, S. (2023). Investigating the efficiency and optimization of germanium-based perovskite solar cell using SCAPS 1D. *Indian Journal of Engineering and Materials Sciences (IJEMS)*, *30*(5), 706-712. https://doi.org/10.56042/ijems.v30i5.6863

[39] Bhujbal, P. K., Sakunde, B., Supekar, A., Bh, H., Saini, S., Dhirhe, D. & Pathan, H. M. (2024). Unlocking the potential of WS2 as an electron transport layer in lead-free methylammonium tin iodide-based perovskite solar cells: a comprehensive defect study using the SCAPS-1D framework. ES Energy & Environment, 26, 1225. http://dx.doi.org/10.30919/esee1225

[40] Ijam, A. (2025). Design and Assessment of the Electrical Characteristics of Cs2AgBi0. 75Sb0. 25Br6 Perovskite Solar Cell: A Numerical Study. Results in Engineering, 105180. https://doi.org/10.1016/j.rineng.2025.105180

[41] Jaiswal, N., Kumari, D., Shukla, R., & Pandey, S. K. (2023). Design and performance optimization of eco-friendly Cs2AgBiBr6 double perovskite solar cell. *Journal of Electronic Materials*, *52*(12), 7842-7849. https://doi.org/10.1007/s11664-023-10705-2

[42] Islam, M. A., Abou Hashish, M. D., Hatta, S. M., Soin, N. B., Khan, S., & Amin, N. (2023, February). Device optimization of a Pb-free all perovskite tandem solar cell with 29.59% power conversion efficiency. In *IOP Conference Series: Materials Science and Engineering* (Vol. 1278, No. 1, p. 012005). IOP Publishing. https://doi.org/10.1088/1757-899X/1278/1/012005

[43] Almahsen, S. B., & Al-Dahash, G. A. (2025). High-efficiency lead-free all-perovskite tandem solar cells achieving 28.22% power conversion efficiency: A Cs2AgBi0. 75Sb0. 25Br6/FASnI3 heterostructure design. *Results in Optics*, 100882. https://doi.org/10.1016/j.rio.2025.100882